Nonlinear effects in the response of a floating ice plate to a moving load

By EMILIAN PĂRĂU[1,2] AND FREDERIC DIAS[3]

[1]Institut Non Linéaire de Nice, Nice, France
[2]Faculty of Mathematics, West University of Timişoara, Timişoara, Romania
[3]Centre de Mathématiques et de Leurs Applications
Ecole Normale Supérieure de Cachan, France

The steady response of an infinite unbroken floating ice sheet to a moving load is considered. It is assumed that the ice sheet is supported below by water of finite uniform depth. For a concentrated line load, earlier studies based on the linearization of the problem have shown that there are two 'critical' load speeds near which the steady deflection is unbounded. These two speeds are the speed c_0 of gravity waves on shallow water and the minimum phase speed $c_{\min}$. Since deflections cannot become infinite as the load speed approaches a critical speed, Nevel (1970) suggested nonlinear effects, dissipation or inhomogeneity of the ice, as possible explanations. The present study is restricted to the effects of nonlinearity when the load speed is close to $c_{\min}$. A weakly nonlinear analysis, based on dynamical systems theory and on normal forms, is performed. The difference between the critical speed $c_{\min}$ and the load speed U is taken as the bifurcation parameter. The resulting normal form reduces at leading order to a forced nonlinear Schrödinger equation, which can be integrated exactly. It is shown that the water depth plays a role in the effects of nonlinearity. For large enough water depths, ice deflections in the form of solitary waves exist for all speeds up to (and including) $c_{\min}$. For small enough water depths, steady bounded deflections exist only for speeds up to U^*, with $U^* < c_{\min}$. The weakly nonlinear results are validated by comparison with numerical results based on the full governing equations. The model is validated by comparison with experimental results in Antarctica (deep water) and in a lake in Japan (relatively shallow water). Finally, nonlinear effects are compared with dissipation effects. Our main conclusion is that nonlinear effects play a role in the response of a floating ice plate to a load moving at a speed slightly smaller than $c_{\min}$. In deep water, they are a possible explanation for the persistence of bounded ice deflections for load speeds up to $c_{\min}$. In shallow water, there seems to be an apparent contradiction, since bounded ice deflections have been observed for speeds up to $c_{\min}$ while the theoretical results predict bounded ice deflection only for speeds up to $U^* < c_{\min}$. But in practice the value of U^* is so close to the value of $c_{\min}$ that it is difficult to distinguish between these two values.

1. Introduction

The study of the deformation of a floating ice sheet due to a load moving on top of it has several applications, including the use of air-cushioned vehicles to break the ice as described for example in the book by Ashton (1986), and the transformation of bodies of water into roads and runways in winter in many areas as mentioned by

Physical parameters	McMurdo Sound	Lake Saroma
Young's modulus E	$4.2 \times 10^9 \,\mathrm{N\,m^{-2}}$	$5.1 \times 10^8 \,\mathrm{N\,m^{-2}}$
Poisson's ratio v	0.3	0.33
Ice thickness h	1.6 m	0.17 m
Flexural rigidity D	1.6×10^9 Nm	2.35×10^5 Nm
Water depth H	350 m	6.8 m
Load speed U	$0 < U < 28 \,\mathrm{m\,s^{-1}}$	$0 < U < 14 \,\mathrm{m\,s^{-1}}$
Shallow water velocity c_0	$59 \,\mathrm{m\,s^{-1}}$	$8.2 \,\mathrm{m\,s^{-1}}$
Minimum wave velocity $c_{\min}$	$18 \,\mathrm{m\,s^{-1}}$	$6.09 \,\mathrm{m\,s^{-1}}$
Wavenumber $k_{\min}$	$0.039 \,\mathrm{m^{-1}}$	$0.334 \,\mathrm{m^{-1}}$
Wavenumber k^*	$0.129 \,\mathrm{m^{-1}}$	$0.6 \,\mathrm{m^{-1}}$
Water density ρ	$1024 \,\mathrm{kg\,m^{-3}}$	$1026 \,\mathrm{kg\,m^{-3}}$
Ice density ρ'	$917 \,\mathrm{kg\,m^{-3}}$	

TABLE 1. Physical parameters for two sets of experiments: McMurdo Sound in Antarctica (Squire *et al.* 1988) and Lake Saroma in Hokkaido, Japan (Takizawa 1985, 1987, 1988).

Milinazzo, Shinbrot & Evans (1995). The recent monograph by Squire *et al.* (1996) is devoted to the rich topic of moving loads on ice plates. Many features of the response of the ice sheet can be explained by modelling the ice as a thin elastic plate. This classical model leads to the following flexural–gravity free wave dispersion relation:

$$c(k)^2 = \left(\frac{g}{k} + \frac{Dk^3}{\rho} \right) \tanh(kH), \quad \text{where } D = \frac{Eh^3}{12(1 - v^2)}. \tag{1.1}$$

Here, k is the wavenumber, c the wave speed, g the acceleration due to gravity, ρ the density of water, H the water depth, D the flexural rigidity of ice, h the ice thickness, E denotes Young's modulus and v Poisson's ratio for ice.

This model has been used successfully by Nevel (1970), Davys, Hosking & Sneyd (1985), Schulkes & Sneyd (1988) and Milinazzo *et al.* (1995). However, as pointed out by Strathdee, Robinson & Haines (1991), this model may be unsatisfactory in certain conditions. The limits of the model will be discussed in §2.

In this paper, two sets of experimental data will be used for reference: experiments in McMurdo Sound in Antarctica (Squire *et al.* 1988) and in Lake Saroma in Hokkaido, Japan (Takizawa 1985, 1987, 1988). Typical values of the physical parameters involved in these experiments are summarized in table 1. Equation (1.1) is plotted in figure 1 for the conditions of Takizawa's experiments in Lake Saroma as well as for the conditions in McMurdo Sound.

A trivial property of the dispersion relation (1.1) is that it exhibits a minimum, whatever the values of the physical parameters are. For McMurdo Sound, this minimum is reached at $k = 0.039 \,\mathrm{m^{-1}}$ (i.e. a wavelength of 161 m). For Lake Saroma, it is reached at $k = 0.334 \,\mathrm{m^{-1}}$ (i.e. a wavelength of 18.8 m). The corresponding speeds and frequencies are $c = 18 \,\mathrm{m\,s^{-1}}$ and $f = 0.11$ Hz for McMurdo Sound and $c = 6.09 \,\mathrm{m\,s^{-1}}$ and $f = 0.32$ Hz for Lake Saroma.

The presence of the minimum leads to a failure of linearized versions of the problem. Assume a load moving at a constant speed U from right to left along the ice sheet and linearize the equations in the frame of reference moving with the load. For $U < c_{\min}$ the solution tends to a uniform flow with constant velocity U at infinity, while for $c_0 > U > c_{\min}$, the solution of the linearized equations is characterized by trains of waves in the far field (gravity waves downstream with wavenumber k_g
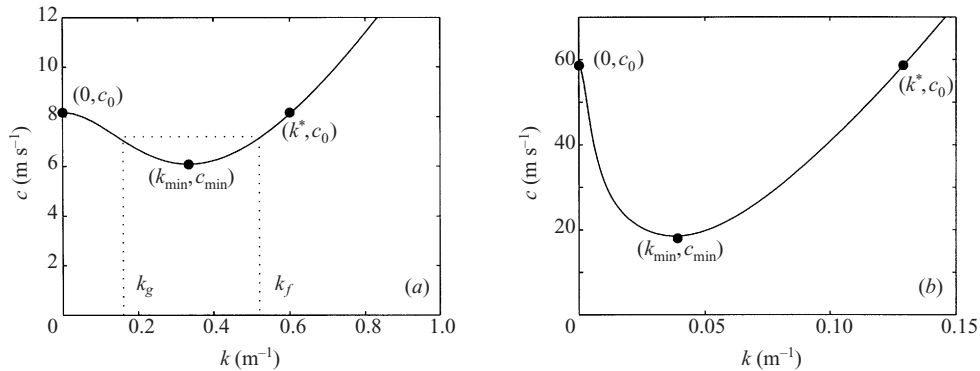
FIGURE 1. Phase velocity c versus wavenumber k for the parameters corresponding to the experiments in: (a) Takizawa (1985), (b) Squire *et al.* (1988). Three regimes can be identified depending on the load speed U: the single wave stage when $U > c_0$ (the wavenumber of the single wave is larger than k^*), the two-wave stage when $c_{min} < U < c_0$ (the wavenumbers of the two waves are k_g on the gravity side and k_f on the flexural side), and the 'solitary' wave stage when $U < c_{min}$. The values of c_0, c_{min}, k^* and k_{min} are given in table 1.

and flexural waves upstream with wavenumber k_f – see figure 1). The amplitude of the periodic waves being proportional to $1/(k_f - k_g)$, the linearization fails in the neighbourhood of $U = c_{min}$. According to Squire *et al.* (1996), the linearized problem was first solved by Kheysin (1963).

Since deflections clearly cannot become infinite as the load speed approaches c_{min}, possible explanations are the effects of nonlinearity or dissipation. In this paper we focus on the effects of nonlinearity. Note that a similar situation occurs for capillary–gravity waves. For historical reasons the problem of capillary–gravity waves has been studied more extensively than the problem of flexural–gravity waves and several recent theoretical studies have been devoted to the effects of nonlinearity on capillary–gravity waves travelling at speeds close to c_{min} (see for example Dias & Kharif 1999 for a review). Unfortunately, although some attempts have been made (see Longuet-Higgins & Zhang 1997), experiments on capillary–gravity waves travelling at speeds close to c_{min} are difficult to perform. For flexural–gravity waves, the situation is the opposite. Experimental results are available but the nonlinear theory has not yet been developed.

The paper is organized as follows. After formulating the problem in §2, the problem is linearized in §3 and results on the linearized problem are recalled. In §4, we add nonlinear terms in order to study solutions with load speeds close to c_{min}. The analysis, which is performed in a frame of reference moving with the load, is based on dynamical systems theory and gives at leading order a forced nonlinear Schrödinger (NLS) equation for the envelope A of the ice-sheet deflection,

$$A_{xx} = q_1 \mu A - q_2 A |A|^2 + \epsilon \delta, \tag{1.2}$$

where x is the horizontal coordinate, q_1 and q_2 are coefficients depending on the water depth, μ is proportional to the difference $c_{min} - U$, ϵ is proportional the load-induced pressure and δ is the Dirac delta function. In water of depth H, the ice-sheet deflection $\zeta(x)$ is given by

$$\zeta(x) = \frac{\tanh(k_{min}H)}{k_{min}}(A e^{ik_{min}x} + \text{c.c.}),$$
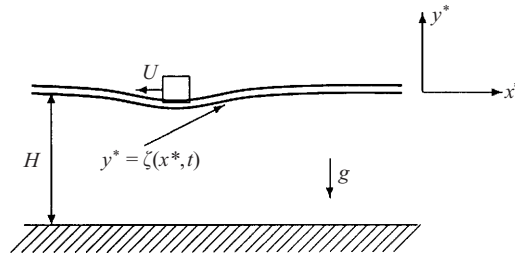
FIGURE 2. Sketch of the flow. A load is moving at speed U from right to left on top of the ice sheet.

where c.c. stands for complex conjugate and A is a solution of equation (1.2). In §5, the forced NLS equation (1.2) is integrated. It is shown that the water depth plays a crucial role in the effects of nonlinearity. For small enough water depths, steady bounded deflections exist only for speeds up to U^*, with $U^* < c_{\min}$. For large enough water depths, ice deflections in the form of solitary waves exist for all speeds up to (and including) $c_{\min}$. In particular, for great depth, solutions

$$\zeta(x) = 2k_{\min}^{-1} s(x) \cos(k_{\min}x),$$

with

$$s(x) = -\sqrt{\frac{2\mu q_1}{|q_2|}} \left(\frac{1}{\sinh(\sqrt{\mu q_1}|x| + \alpha)} \right),$$

are found. The coefficients q_1 and q_2 are equal respectively to 0.42 and -0.24, while α is the solution of the equation

$$\frac{\cosh \alpha}{\sinh^2 \alpha} = \frac{\sqrt{|q_2|}}{2\sqrt{2}q_1} \left(\frac{\epsilon}{\mu} \right).$$

Then a comparison is made between theory and experiments. Dissipative effects are discussed. In the Appendix numerical results based on the full equations are presented.

2. Formulation of the problem

A two-dimensional layer of a fluid of finite depth H beneath an ice sheet of thickness h is considered. The sketch of the flow is shown in figure 2. The fluid is assumed to be inviscid and incompressible and the flow irrotational. We introduce Cartesian coordinates with the x^*-axis being the bottom of the ice sheet at rest and the y^*-axis directed vertically upwards. The vertical ice-sheet deflection is denoted by $y^* = \zeta(x^*, t)$. The velocity components are denoted by u^* (horizontal) and v^* (vertical).

The equations of motion inside the fluid domain are

$$\frac{\partial u^*}{\partial x^*} + \frac{\partial v^*}{\partial y^*} = 0, \quad \frac{\partial u^*}{\partial y^*} - \frac{\partial v^*}{\partial x^*} = 0 \quad \text{for } (x^*, y^*) \in \mathbb{R} \times (-H, \zeta(x^*, t)).$$

The boundary condition at the bottom is $v^* = 0$ at $y^* = -H$. Along the bottom of the ice sheet $y^* = \zeta(x^*, t)$, the kinematic condition $\zeta_t + u^* \zeta_{x^*} - v^* = 0$ and the dynamic condition must be satisfied. The dynamic condition depends on the model used to describe the ice. The modelling of ice is a complex topic and we refer to Squire *et al.* (1996) for a review of various models. Here we assume that the terms

involving ice thickness and damping can be neglected. There are several justifications for this. Hosking, Sneyd & Waugh (1988) considered the effects of damping. They used viscoelastic theory to describe the response of a floating ice sheet to a moving vehicle. Takizawa (1987) also discussed briefly the effects of viscoelasticity on ice deflection, by simply assuming that the damping force is proportional to the vertical velocity (viscous damping). Hosking *et al.* adopted a two-parameter memory function to describe the behaviour of the ice. They found that viscoelastic dissipation produces an asymmetric quasi-static response when the vehicle speed U is less than c_{min}, and a finite response at $U = c_{min}$. The damping is more important for the flexural wave than for the gravity wave. Their main conclusion is that many experimental results on ice waves can be explained by assuming a thin elastic plate but that certain features are not satisfactorily described by the elastic theory, such as the observed lag of the position of maximum depression immediately behind the source and the damping of flexural waves. Strathdee *et al.* (1991) considered the effects of ice thickness and discussed the circumstances in which the classical thin-plate theory can be recovered. In the thin-plate approximation, waves of length comparable with or smaller than the plate thickness are neglected. Strathdee *et al.* showed that the thin-plate approximation is mathematically consistent when

$$(1 - v)\frac{\rho g h}{G} \ll 1,$$

where G is the shear modulus. For example, for the Antarctic experiments, this coefficient is of the order of 10^{-6}. Their calculations for stationary loads indicated that thin-plate theory is accurate to within 5% for distances greater than twenty times the ice thickness.

The main contribution of the present paper is to discuss nonlinear effects. But it is not obvious how nonlinearity can be introduced. There are in fact three possibilities, since nonlinear effects can be included in the plate equation as well as in the fluid layer: nonlinear plate–nonlinear flow, linear plate–nonlinear flow, nonlinear plate–linear flow. In a slightly different context (the study of the nonlinear stability of a fluid-loaded elastic plate), Peake (2001) provides an illuminating discussion on these three choices. Following his approach (see his equation (2.1)) as well as the approach of Forbes (1986) (see his equation (2.11)) and Il'ichev (2000) (see his equation (4.1)), who model the ice sheet as a Kirchhoff–Love plate, we include the full nonlinear expression for the plate curvature in the elastic term and for the calculation of the hydrodynamic pressure on the plate. Using the (nonlinear) Bernoulli equation, the dynamic condition becomes

$$\rho\phi_t^* + \tfrac{1}{2}\rho(u^{*2} + v^{*2}) + \rho g\zeta + D\partial_{x^*x^*}^2 \frac{\zeta_{x^*x^*}}{(1 + \zeta_{x^*}^2)^{3/2}} = -p(x^*, t), \qquad (2.1)$$

where ϕ^* is the fluid velocity potential, and $p(x^*, t)$ the pressure distribution exerted by the load on the ice sheet. In (2.1), the tension of the pre-stressed state in the elastic plate has been neglected. Taking it into account would lead to an additional term similar to the surface tension term for capillary–gravity waves. This section would not be complete without mentioning that the inertia of the thin plate has been neglected, compared to the inertia of the moving fluid layer. The plate acceleration is measured by the term $\rho' k h/\rho$. If it is much less than 1, the plate acceleration can be neglected (see Squire *et al.* 1996). In both sets of experiments, this term is of the order of 5% when $k = k_{min}$.

3. Linearized problem

The concentrated load is assumed to be applied at time $t = 0$ and then to move from right to left at a constant speed U. Therefore $p(x^*, t)$ has the form $P\delta(x^* + Ut)\mathscr{H}(t)$, where P is a constant, δ the Dirac delta function and $\mathscr{H}$ the Heaviside step function.

The linearized problem was treated by Schulkes & Sneyd (1988). Some results are recalled here. The linearized dynamic condition (2.1) at the interface is

$$\rho\phi_t^*|_{y^*=0} + \rho g\zeta + D\zeta_{x^*x^*x^*x^*} = -p(x^*, t), \tag{3.1}$$

and the kinematic conditions are

$$\phi_{y^*}^*|_{y^*=-H} = 0, \quad \phi_{y^*}^*|_{y^*=0} = \zeta_t. \tag{3.2}$$

The solution of this problem can be put in the form

$$\zeta(X, t) = \frac{P}{2\pi\rho}(I_1 + I_2 - I_0), \tag{3.3}$$

with

$$I_0 = \int_{-\infty}^{\infty} \frac{e^{ikX}}{\omega_1(k)\omega_2(k)} k \tanh(kH)\,dk, \quad I_1 = \int_{-\infty}^{\infty} \frac{e^{i(kX-\omega_1(k)t)}}{2c(k)\omega_1(k)} \tanh(kH)\,dk,$$

$$I_2 = \int_{-\infty}^{\infty} \frac{e^{i(kX+\omega_2(k)t)}}{2c(k)\omega_2(k)} \tanh(kH)\,dk, \quad \text{and} \quad X = x^* + Ut.$$

The speed $c(k)$ is given by equation (1.1), while $\omega_1(k)$ and $\omega_2(k)$ are defined as follows:

$$\omega_1(k) = k[c(k) + U], \quad \omega_2(k) = k[c(k) - U]. $$

As mentioned above, $c(k)$ has a minimum denoted by $c_{\min}$.

The steady part of the solution is given by $\zeta_s = -(P/2\pi\rho)I_0$. Schulkes & Sneyd (1988) showed that, for $U < c_{\min}$, $I_1, I_2 \to 0$ as $t \to \infty$, so the disturbance approaches a steady state. The integral I_0 can be computed using fast Fourier transforms. It can be shown that the maximum ice deflection $\zeta_{\max}$ occurs at $X = 0$ and that it increases with U. As $U \to c_{\min}$, it becomes infinite. In infinite depth, the expression for $\zeta_{\max}$ is rather simple:

$$\zeta_{\max} = -\frac{P}{\pi\rho}\int_0^{\infty} \frac{dk}{g + Dk^4/\rho - U^2 k}. \tag{3.4}$$

When $U = 0$, it is equal to $-(P/8D)(4D/\rho g)^{3/4}$. Figure 3 shows a plot of $\zeta_{\max} = \zeta_s(0)$ for the Antarctic experiments.

Figure 4 shows the steady ice displacement ζ_s for some load speeds $U < c_{\min}$ ($c_{\min} = 6.09\,\text{m s}^{-1}$) for the physical parameters corresponding to the experiments in Lake Saroma. The linear results are in good agreement with the experimental results, at least for the three speeds $U = 2.2, 4.2$ and $5.5\,\text{m s}^{-1}$ (compare the profiles shown in figure 4 with those in figure 6 of Takizawa (1987) or in figure 1 of Takizawa (1988)). Since the experiments were performed with a rectangular load, our estimate of P, $P = 320\,\text{N/m}$, is rather rough. Clearly, deflections cannot become infinite as the load speed approaches $c_{\min}$. Nevel (1970) suggested nonlinear effects, dissipation or inhomogeneity of the ice, as possible explanations. In the next sections we consider the effects of nonlinearity when the load speed is close to $c_{\min}$.
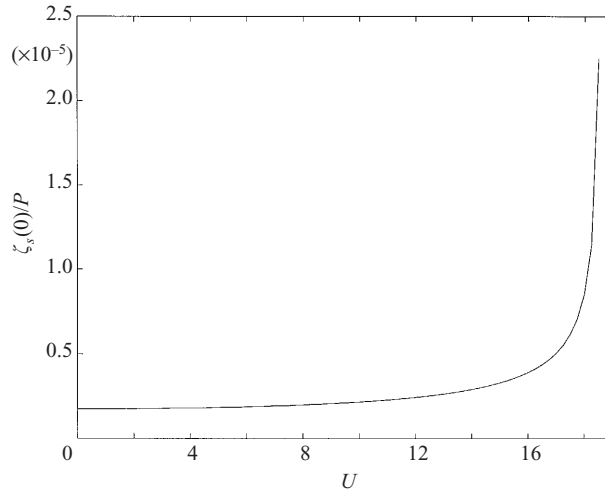
FIGURE 3. Plot of the maximum ice-sheet deflection (3.4) as a function of the load speed U (in $\mathrm{m\,s^{-1}}$) for the physical parameters corresponding to the Antarctic experiments. Since P can only be roughly estimated, the ice deflection has been divided by P. The units of $\zeta_{\max}/P$ are $\mathrm{m^2\,N^{-1}}$. The plot is restricted to speed values between 0 and $c_{\min}$ ($c_{\min} \approx 18\,\mathrm{m\,s^{-1}}$).

4. Dynamical system analysis

Since the load is assumed to move at a constant velocity U, the analysis is for a frame moving from right to left at the velocity U. It is further assumed that the load has been moving for a sufficient length of time that all transient motions of the ice–water system have disappeared, and only the steady motion remains. Dimensionless variables are introduced by taking U as unit velocity and $L = (D/\rho U^2)^{1/3}$ as unit length. At the critical speed $c_{\min}$, L is of the order of 1.8 m for the experiments in Japan and 16.9 m for the Antarctic experiments. The dimensionless parameters are chosen to be

$$\lambda = \frac{gH}{U^2} \quad \text{and} \quad f = \frac{g}{U^2}\left(\frac{D}{\rho U^2}\right)^{1/3}.$$

A summary of the physical quantities as well as the dimensionless quantities is provided in tables 2 and 3.

The problem in dimensionless form reads

$$\phi_{xx} + \phi_{yy} = 0, \quad (x,y) \in \mathbb{R} \times [-\lambda/f, \eta(x)], \tag{4.1}$$

with the boundary conditions

$$v = 0 \quad \text{at } y = -\lambda/f, \tag{4.2}$$

$$u\eta_x - v = 0 \quad \text{at } y = \eta(x), \tag{4.3}$$

$$\tfrac{1}{2}(u^2 + v^2 - 1) + f\eta + \partial_{xx}^2 \frac{\eta_{xx}}{(1+\eta_x^2)^{3/2}} + \varepsilon p_0 = 0 \quad \text{at } y = \eta(x). \tag{4.4}$$

The term $\varepsilon p_0(x)$ denotes the dimensionless pressure due to the moving load. The function p_0 is of compact support.

The change of coordinates introduced by Levi-Civita (1925) is used: the new unknown is $\alpha + i\beta$ as an analytic function of the complex potential $\mathscr{F} = \phi + i\psi$, where

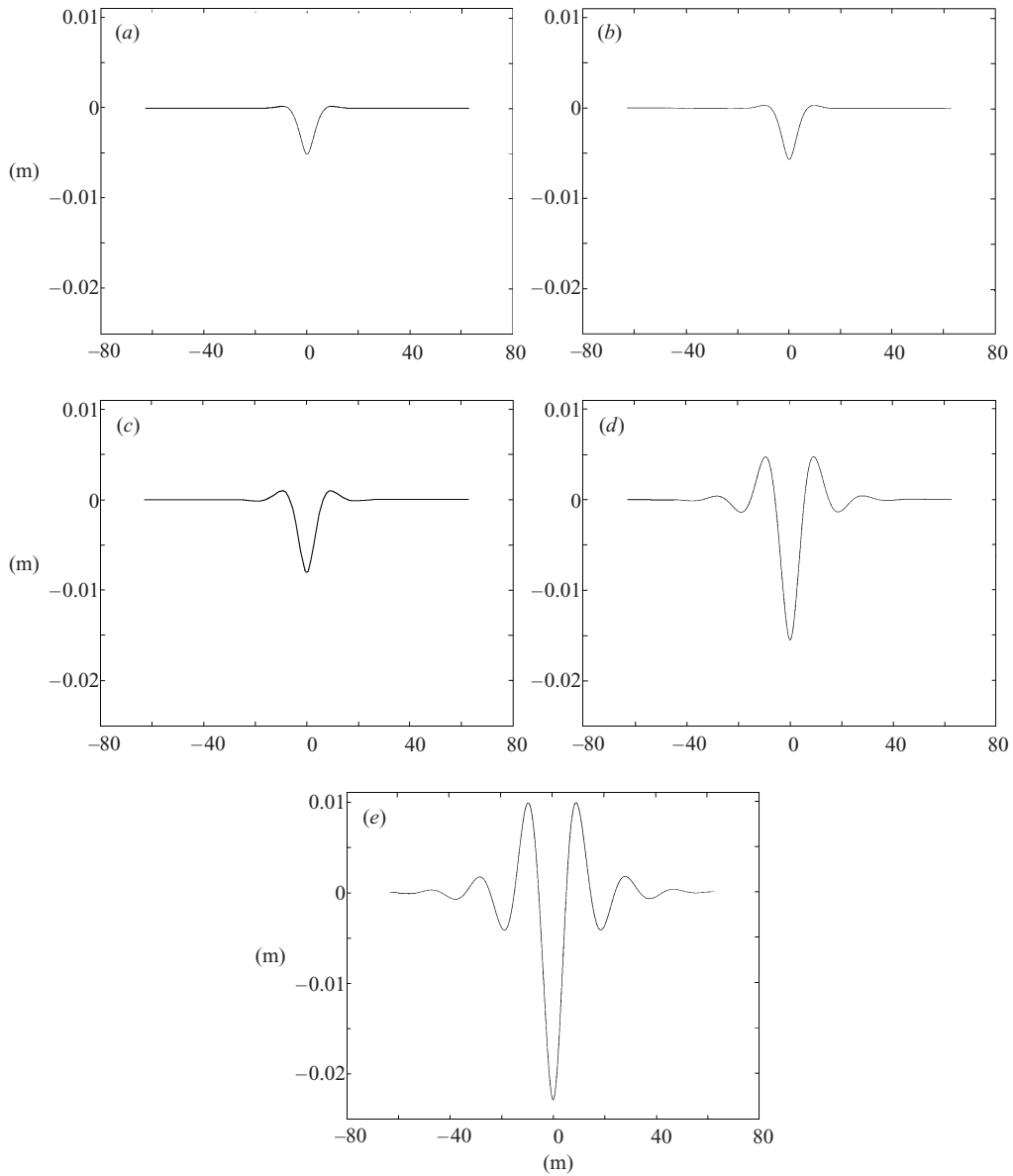$$e^{\beta - i\alpha} \equiv u - iv = \mathscr{F}'(x + iy).$$

FIGURE 4. The steady ice displacement $\zeta(x^* + Ut)$ for the physical parameters corresponding to Takizawa's experiments (see table 1). The value of P has been estimated at $P = 320\,\mathrm{N\,m^{-1}}$. The values of the speed U are 0, 2.2, 4.2, 5.5, 5.8 m s^{-1} in (a)–(e) respectively. Recall that $c_{\min} = 6.09\,\mathrm{m\,s^{-1}}$.

The bottom of the ice sheet is given by $\psi = 0$ and the bottom of the water layer by $\psi = -\lambda/f$. The function α represents the angle of the streamline with the horizontal, while β represents the logarithm of the velocity modulus. In these new coordinates, the system (4.1)–(4.4) can be rewritten as a dynamical system in ϕ. The deflection $\eta(\phi)$ of the ice sheet can be expressed in terms of the new variables as

$$\eta = \int_{-\lambda/f}^{0} (\mathrm{e}^{-\beta}\cos\alpha - 1)\mathrm{d}\psi \quad \text{or} \quad \eta = \frac{\lambda}{f}[\mathrm{e}^{-\beta}\cos\alpha - 1], \tag{4.5}$$

Symbol	Physical quantity	Dimension
t	Time	$[T]$
U	Load velocity	$[L][T]^{-1}$
g	Acceleration due to gravity	$[L][T]^{-2}$
H	Mean water depth	$[L]$
h	Ice sheet thickness	$[L]$
D	Flexural rigidity	$[M][L]^2[T]^{-2}$
E	Young's modulus	$[M][L]^{-1}[T]^{-2}$
k	Wavenumber	$[L]^{-1}$
ρ	Water density	$[M][L]^{-3}$
P	Pressure load	$[M][T]^{-2}$
L	Unit length $(D/\rho U^2)^{1/3}$	$[L]$
(x^*, y^*)	Physical coordinates	$[L]$
(u^*, v^*)	Velocity components	$[L][T]^{-1}$
$\psi^*(x^*, y^*)$	Stream function	$[L]^2[T]^{-1}$
$\phi^*(x^*, y^*)$	Velocity potential	$[L]^2[T]^{-1}$
$\zeta(x^*, t)$	Deflection of the ice sheet	$[L]$

TABLE 2. Physical parameters and their dimension

Symbol	Definition	Dimensionless quantity
v		Poisson's ratio
κ	kH	Dimensionless wavenumber based on water depth
K	kL	Dimensionless wavenumber based on unit length
f	gL/U^2	Inverse square Froude number based on L
λ	gH/U^2	Inverse square Froude number based on H
x	$(x^* + Ut)/L$	Dimensionless horizontal coordinate in moving frame
y	y^*/L	Dimensionless vertical coordinate
(u, v)	$(u^*, v^*)/U$	Dimensionless velocity components
η	ζ/L	Dimensionless deflection of the ice sheet
(ϕ, ψ)	$(\phi^*, \psi^*)/UL$	Dimensionless potential and streamfunction
$\mathscr{F}$	$\phi + \mathrm{i}\psi$	Dimensionless complex potential

TABLE 3. Dimensionless quantities

where [ ] denotes the mean value of enclosed term over the interval $[-\lambda/f, 0]$. Since α and β are small, one can expand η as follows:

$$\eta = \frac{\lambda}{f}(-[\beta] + \cdots). \tag{4.6}$$

Let $\alpha_0(\phi) = \alpha(\phi, 0), \beta_0(\phi) = \beta(\phi, 0)$. Define

$$V = \mathrm{e}^{\beta_0}\frac{\partial\alpha_0}{\partial\phi}, \quad W = \left(\frac{\mathrm{e}^{\beta_0}}{\cos\alpha_0}\right)\frac{\partial V}{\partial\phi}. \tag{4.7}$$

Then one can replace the system (4.1)–(4.4) by the system

$$\frac{\partial}{\partial\phi}\begin{pmatrix}\alpha_0 \\ V \\ W \\ \alpha \\ \beta\end{pmatrix} = \begin{pmatrix}V\mathrm{e}^{-\beta_0} \\ W\mathrm{e}^{-\beta_0}\cos\alpha_0 \\ \cos\alpha_0(-\sinh\beta_0 - \lambda\mathrm{e}^{-\beta_0}[\mathrm{e}^{-\beta}\cos\alpha - 1] - \varepsilon p_0\mathrm{e}^{-\beta_0}) \\ \beta_\psi \\ -\alpha_\psi\end{pmatrix} \tag{4.8}$$

with the boundary condition $\alpha(\phi, -\lambda/f) = 0$. The first and second equations in (4.8)

are the definitions (4.7). The third equation is Bernoulli's equation, the fourth and the fifth are the Cauchy–Riemann equations. See Dias & Iooss (2003) for details.

The forcing term εp_0 is temporarily set equal to zero. It will be reintroduced later on. When $\varepsilon = 0$, the right-hand side of the system (4.8) anticommutes with $R = \text{diag}(-1, 1, -1, -1, 1)$. In other words, if the vector $(\alpha_0(\phi), V(\phi), W(\phi), \alpha(\phi, \psi), \beta(\phi, \psi))$ is a solution of the system (4.8), then $(-\alpha_0(-\phi), V(-\phi), -W(-\phi), -\alpha(-\phi, \psi), \beta(-\phi, \psi))$ is also a solution of the system.

Introducing the notation $\boldsymbol{w} = (\alpha_0, V, W, \alpha, \beta)^T$, system (4.8) can be viewed as a 'spatial' dynamical system

$$\mathbf{w}_\phi = \mathrm{L}\boldsymbol{w} + \mathrm{N}(\boldsymbol{w}), \tag{4.9}$$

where L is the linearization about $\boldsymbol{w} = 0$ of the right-hand side of the system and $\mathrm{N}(\boldsymbol{w})$ is the nonlinear part of the system. The operator L acts on $\boldsymbol{w}$ as follows:

$$\mathrm{L}\boldsymbol{w} = \begin{pmatrix} V \\ W \\ -\beta_0 + \lambda[\beta] \\ \beta_\psi \\ -\alpha_\psi \end{pmatrix}.$$

In order to find the spectrum of L, let us solve the linearized problem $\mathrm{L}\boldsymbol{w} = \sigma\boldsymbol{w}$. It is easy to show that the spectrum of L consists only of eigenvalues σ, which satisfy the equation

$$(\sigma^4 + f)\sin\left(\frac{\lambda}{f}\sigma\right) = \sigma\cos\left(\frac{\lambda}{f}\sigma\right). \tag{4.10}$$

When $\sigma = \pm\mathrm{i}(f/\lambda)\kappa$, equation (4.10) becomes the dispersion relation (1.1). The reversibility of the system implies that if σ is an eigenvalue, then $-\sigma, \bar{\sigma}, -\bar{\sigma}$ are eigenvalues as well. Moreover, $\sigma = 0$ is an eigenvalue if and only if $\lambda = 1$. The behaviour of the eigenvalues close to the imaginary axis is shown in figure 5 in the parameter space (f, λ).

From now on, the analysis is restricted to values of f and λ close to the curve Γ in the (f, λ)-plane (the solid line in figure 5), defined by the existence of a pair of double imaginary eigenvalues $\sigma = \pm\mathrm{i}(f/\lambda)\kappa$ (the so-called 1:1 resonance). These imaginary eigenvalues, which correspond to the minimum of the dispersion curve (1.1), that is $\pm\mathrm{i}(f/\lambda)\kappa = \pm\mathrm{i}k_{\min}L$, satisfy the relation (4.10), rewritten as

$$D(\kappa; \lambda, f) \equiv \left[\kappa^4\left(\frac{f}{\lambda}\right)^3 + \lambda\right]\tanh\kappa - \kappa = 0, \tag{4.11}$$

as well as the equation

$$\frac{\partial D}{\partial \kappa} = 4\kappa^3\left(\frac{f}{\lambda}\right)^3\tanh\kappa + \left[\kappa^4\left(\frac{f}{\lambda}\right)^3 + \lambda\right](1 - \tanh^2\kappa) - 1 = 0. \tag{4.12}$$

The parametric form of Γ is given by

$$\left.\begin{aligned} f &= \frac{3\tanh\kappa + \kappa - \kappa\tanh^2\kappa}{4\tanh^2\kappa}\left(\frac{\tanh\kappa - \kappa + \kappa\tanh^2\kappa}{4\tanh^2\kappa}\right)^{1/3}, \\ \lambda &= \frac{\kappa(3\tanh\kappa + \kappa - \kappa\tanh^2\kappa)}{4\tanh^2\kappa}, \end{aligned}\right\} \tag{4.13}$$
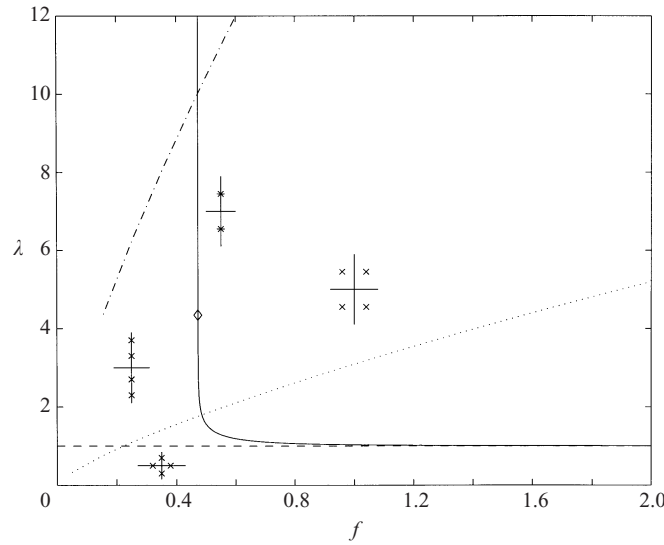
FIGURE 5. The solid line is the set of values of f and λ corresponding to the minimum of the dispersion curve, given in parametric form by equation (4.13). The dashed line $\lambda = 1$ corresponds to the speed of waves on shallow water $\sqrt{gH}$. The change in behaviour of the eigenvalues close to the imaginary axis is indicated. The experimental values are given by $\lambda = (\rho g H^4/D)^{1/4} f^{3/4}$, i.e. $\lambda \approx 3.09 f^{3/4}$ for Takizawa's experiments (dotted line) and $\lambda \approx 17.58 f^{3/4}$ for the McMurdo experiments (dashed-dotted line). The diamond represents the vanishing of the coefficient q_2 given by equation (4.30).

for $\kappa \in (0, \infty)$. Recall that κ is equal to $k_{\min} H$. The asymptotic behaviours of f and λ are

$$f \sim (6\kappa^2)^{-1/3} + O(\kappa^{4/3}), \quad \lambda \sim 1 + \tfrac{1}{6}\kappa^2 + O(\kappa^4), \quad \text{as } \kappa \to 0$$

and

$$f \sim \frac{3}{4^{4/3}} + 2^{1/3}\mathrm{e}^{-2\kappa}, \quad \lambda \sim \tfrac{3}{4}\kappa \quad \text{as } \kappa \to \infty.$$

In infinite depth ($\kappa \to \infty$), $f \approx 0.4725$. For the physical parameters corresponding to Takizawa's experiments, $\kappa = 2.27$ and (4.13) gives $(f, \lambda) = (0.485, 1.8)$. For the McMurdo experiments, $\kappa = 13.65$ and (4.13) gives $f \approx 0.48$ and $\lambda \approx 10$.

Since we look for solutions with (f, λ) close to the curve Γ, we define a small parameter

$$\mu = (f^*/\lambda^*)(\lambda - \lambda^*), \tag{4.14}$$

where the point (f^*, λ^*) belongs to the curve Γ given by (4.13). The parameter μ is proportional to $c_{\min} - U$. In the remainder of this section, we will drop the stars whenever there is no possible confusion. We will also use the notation $K = \kappa f/\lambda$.

The double eigenvalues $\pm iK$ are non-semi-simple. The eigenvectors φ_0^+ (resp. φ_0^-) and generalized eigenvectors φ_1^+ (resp. φ_1^-), corresponding to the eigenvalue $+iK$ (resp. $-iK$), are

$$\varphi_0^+ = \frac{1}{\cosh \kappa} \begin{pmatrix} \mathrm{i} \sinh \kappa \\ -K \sinh \kappa \\ -\mathrm{i} K^2 \sinh \kappa \\ \mathrm{i} \sinh(K\psi + \kappa) \\ -\cosh(K\psi + \kappa) \end{pmatrix}, \quad \varphi_0^- = \overline{\varphi_0^+}, \tag{4.15}$$

$$\boldsymbol{\varphi}_1^+ = \frac{1}{\cosh \kappa} \begin{pmatrix} 0 \\ \mathrm{i} \sinh \kappa \\ -2K \sinh \kappa \\ \psi \cosh(K\psi + \kappa) - (\lambda/f) \sinh(K\psi)/\sinh \kappa \\ \mathrm{i}[\psi \sinh(K\psi + \kappa) - (\lambda/f) \cosh(K\psi)/\sinh \kappa] \end{pmatrix}, \quad \boldsymbol{\varphi}_1^- = \overline{\boldsymbol{\varphi}_1^+}. \quad (4.16)$$

Let us now reintroduce the forcing term εp_0. The method described by Il'ichev (2000) for the case $\varepsilon = 0$, which is based on the centre manifold reduction theorem, is extended to the case $\varepsilon \neq 0$. This means that all solutions of (4.9), staying small and bounded for $\phi \in (-\infty, +\infty)$, can be written in the form

$$\boldsymbol{w} = A(\phi)\boldsymbol{\varphi}_0^+ + B(\phi)\boldsymbol{\varphi}_1^+ + \bar{A}(\phi)\boldsymbol{\varphi}_0^- + \bar{B}(\phi)\boldsymbol{\varphi}_1^- + \Phi(\mu, \varepsilon; A, B, \bar{A}, \bar{B}), \qquad (4.17)$$

where $\Phi(0, 0; A, B, \bar{A}, \bar{B})$ is a nonlinear function containing the higher-order terms in $A, B, \bar{A}, \bar{B}$.

A powerful method for finding A and B consists of using normal form theory. Combining the normal form theory described by Iooss & Adelmeyer (1992) for $\varepsilon = 0$ (1:1 resonance normal form with reversibility) and the method used by Kirchgässner (1988) and Mielke (1986) for the case $\varepsilon \neq 0$, Părău & Dias (2000) showed that the reduced ordinary differential equations resulting from the centre manifold reduction can be put in the form

$$A_\phi = \mathrm{i}KA + B + \mathrm{i}AP(\mu; |A|^2, \tfrac{1}{2}\mathrm{i}(A\bar{B} - \bar{A}B)) - \mathrm{i}\varepsilon p_0 \mathscr{C}_0 \mathscr{C}_1 + \cdots, \qquad (4.18)$$

$$B_\phi = \mathrm{i}KB + \mathrm{i}BP(\mu; |A|^2, \tfrac{1}{2}\mathrm{i}(A\bar{B} - \bar{A}B)) + AQ(\mu; |A|^2, \tfrac{1}{2}\mathrm{i}(A\bar{B} - \bar{A}B)) + \varepsilon p_0 \mathscr{C}_0 + \cdots, \qquad (4.19)$$

where P and Q are polynomials defined by

$$P(\mu; |A|^2, \tfrac{1}{2}\mathrm{i}(A\bar{B} - \bar{A}B)) = p_1\mu + p_2|A|^2 + p_3\tfrac{1}{2}\mathrm{i}(A\bar{B} - \bar{A}B) + \cdots,$$
$$Q(\mu; |A|^2, \tfrac{1}{2}\mathrm{i}(A\bar{B} - \bar{A}B)) = q_1\mu - q_2|A|^2 + q_3\tfrac{1}{2}\mathrm{i}(A\bar{B} - \bar{A}B) + \cdots.$$

For our purpose, only the coefficients q_1, q_2 and the constant $\mathscr{C}_0$ are needed. In order to compute them, the forcing term εp_0 is again set equal to zero. We first compute the leading coefficient q_1. It is easy to find, since it is directly related to the eigenvalues of the linearization of (4.18)–(4.19) about (0,0):

$$\sigma = \mathrm{i}\left(\frac{f^*}{\lambda^*}\kappa + p_1\mu\right) \pm \sqrt{q_1}\sqrt{\mu} + O(\mu^{3/2}).$$

If we substitute this expression into (4.10) with $\lambda = \lambda^* + (\lambda^*/f^*)\mu$ and expand in powers of μ, one finds that

$$q_1 = 2^{1/3} \frac{(\sinh \kappa \cosh \kappa - \kappa)^{1/3} \sinh^{7/3} \kappa}{3 \cosh \kappa \sinh^2 \kappa - 2\kappa^2 \cosh \kappa - \kappa \sinh \kappa}.$$

It can be checked that $q_1 > 0$, for all $\kappa \in \mathbb{R}^+$. Its asymptotic behaviour is given by

$$q_1 \sim \frac{1}{4}\left(\frac{6}{\kappa}\right)^{2/3} \quad \text{as } \kappa \to 0 \quad \text{and} \quad q_1 \to \frac{2^{1/3}}{3} \approx 0.42 \text{ as } \kappa \to \infty.$$

Values of q_1 for the experiments in Japan and the Antarctic are given in table 4.

Next we compute the coefficient q_2 by using the method described by Dias & Iooss (1993). Let us set $\mu = 0$ in the following computations since this does not change

	q_1	q_2	$\mathscr{C}_0$	$\mathscr{A}$	Depth (m)	Critical depth (m)
Antarctic experiments	0.42	−0.15	0.29	−0.27	350	152
Experiments in Japan	0.49	1.05	0.29	−0.16	6.8	16.8

TABLE 4. Numerical values of various coefficients appearing in the weakly nonlinear analysis. These coefficients depend on the water depth. The values which are shown correspond to the water depth in the experiments. If the water depth were allowed to vary, the coefficient q_2 would vanish at the critical depth shown.

anything. The nonlinear part of equation (4.9), $\mathrm{N}(w)$, is rewritten as

$$\mathrm{N}(w) = \mathrm{N}_2(w, w) + \mathrm{N}_3(w, w, w) + \cdots, \tag{4.20}$$

where N_2 denotes the quadratic terms

$$\mathrm{N}_2(w, w) = \begin{pmatrix} -V\beta_0 \\ -W\beta_0 \\ \lambda(\frac{1}{2}[\alpha^2] - \frac{1}{2}[\beta^2] - \beta_0[\beta]) \\ 0 \\ 0 \end{pmatrix},$$

and N_3 denotes the cubic terms

$$\mathrm{N}_3(w, w, w) = \begin{pmatrix} \frac{1}{2}V\beta_0^2 \\ \frac{1}{2}W(\beta_0^2 - \alpha_0^2) \\ \frac{1}{2}\lambda(-\alpha_0^2[\beta] + \beta_0^2[\beta] + \beta_0[\beta^2] - \beta_0[\alpha^2] + \frac{1}{3}[\beta^3] - [\beta\alpha^2]) + \frac{1}{2}\beta_0\alpha_0^2 - \frac{1}{6}\beta_0^3 \\ 0 \\ 0 \end{pmatrix}.$$

The dots in (4.20) denote higher-order terms. In addition to (4.9), another expression for w_ϕ can be obtained by differentiating (4.17) with respect to ϕ and setting $\mu = 0$:

$$w_\phi = A_\phi \varphi_0^+ + B_\phi \varphi_1^+ + \bar{A}_\phi \varphi_0^- + \bar{B}_\phi \varphi_1^- + \Phi_\phi(0, 0; A, B, \bar{A}, \bar{B}). \tag{4.21}$$

Next we give the first terms in the expansion of $\Phi(0, 0; A, B, \bar{A}, \bar{B})$:

$$\Phi = (A^2\Phi_{2000} + \text{c.c.}) + |A|^2\Phi_{1100} + (AB\Phi_{1010} + \text{c.c.}) + (\bar{A}B\Phi_{0110} + \text{c.c.}) \\ + (A^3\Phi_{3000} + \text{c.c.}) + |A|^2(A\Phi_{2100} + \text{c.c.}) + \cdots,$$

where c.c. stands for complex conjugate. If A_ϕ and B_ϕ are replaced in (4.21) by their expressions from (4.18) and (4.19), we can equate the powers of A, B and so on in (4.9) and (4.21), which leads to the following system of equations:

$$\mathrm{L}\varphi_0^+ = \mathrm{i}K\varphi_0^+, \tag{4.22}$$

$$\mathrm{L}\varphi_1^+ = \mathrm{i}K\varphi_1^+ + \varphi_0^+, \tag{4.23}$$

$$\mathrm{L}\Phi_{2000} + \mathrm{N}_2(\varphi_0^+, \varphi_0^+) = 2\mathrm{i}K\Phi_{2000}, \tag{4.24}$$

$$\mathrm{L}\Phi_{1100} + 2\mathrm{N}_2(\varphi_0^+, \varphi_0^-) = 0, \tag{4.25}$$

$$\mathrm{L}\Phi_{2100} + 2\mathrm{N}_2(\varphi_0^+, \Phi_{1100}) \\ + 2\mathrm{N}_2(\varphi_0^-, \Phi_{2000}) + 3\mathrm{N}_3(\varphi_0^+, \varphi_0^+, \varphi_0^-) = \mathrm{i}K\Phi_{2100} + \mathrm{i}p_2\varphi_0^+ - q_2\varphi_1^+. \tag{4.26}$$

The adjoint operator L* of L, which is such that

$$\langle Lw, w^* \rangle = \langle w, L^*w^* \rangle, \quad w \in D(L), \quad w^* = (V^*, W^*, \alpha_0^*, \alpha^*, \beta^*)^T \in D(L^*),$$

is introduced. The notation $\langle \cdot, \cdot \rangle$ denotes the scalar product defined as

$$\langle w, w^* \rangle = \alpha_0 \overline{V^*} + V \overline{W^*} + W \overline{\alpha_0^*} + \int_{-\lambda/f}^0 (\alpha \overline{\alpha^*} + \beta \overline{\beta^*}) d\psi.$$

The domains $D(L)$ and $D(L^*)$ are such that they contain the boundary conditions

$$\{\alpha(\cdot, -\lambda/f) = 0, \quad \alpha(\cdot, 0) = \alpha_0\} \quad \text{for } D(L),$$

and

$$\{\alpha^*(\cdot, -\lambda/f) = 0, \quad \alpha^*(\cdot, 0) = \alpha_0^*\} \quad \text{for } D(L^*).$$

The operator L* acts on w^* as

$$L^*w^* = \begin{pmatrix} -\beta^*(\cdot, 0) \\ V^* \\ W^* \\ \beta_\psi^* \\ f\alpha^*(\cdot, 0) - \alpha_\psi^* \end{pmatrix}.$$

The eigenvectors ψ_+^1 and generalized eigenvectors ψ_+^0 for the adjoint operator L* satisfy

$$L^*\psi_+^1 = -iK\psi_+^1, \quad L^*\psi_+^0 = -iK\psi_+^0 + \psi_+^1,$$

and can be chosen so that

$$\langle \varphi_0^+, \psi_+^1 \rangle = 0, \quad \langle \varphi_0^+, \psi_+^0 \rangle = 1, \quad \langle \varphi_1^+, \psi_+^1 \rangle = 1, \quad \langle \varphi_1^+, \psi_+^0 \rangle = 0.$$

One finds that

$$\psi_+^1 = \mathscr{C}_0 \begin{pmatrix} K^2 \\ iK \\ -1 \\ -\sinh(K\psi + \kappa)/\sinh\kappa \\ i[\cosh(K\psi + \kappa)/\sinh\kappa - \lambda/\kappa] \end{pmatrix},$$

where

$$\mathscr{C}_0 = \left(\frac{f}{\lambda}\right)^2 \frac{2\kappa^2 \sinh^2\kappa \cosh\kappa}{3\sinh^2\kappa \cosh\kappa - \kappa \sinh\kappa - 2\kappa^2 \cosh\kappa}. \tag{4.27}$$

Since ψ_+^0 is not needed, we do not provide its expression. The constant $\mathscr{C}_1$ in (4.18) appears in ψ_+^0 but is not needed either. The asymptotic behaviour of $\mathscr{C}_0$ is

$$\mathscr{C}_0 \sim \frac{6^{1/3}}{4}\kappa^{-4/3} + O(\kappa^{2/3}) \text{ as } \kappa \to 0, \quad \mathscr{C}_0 \sim \frac{4^{1/3}}{6} \text{ as } \kappa \to \infty.$$

$\mathscr{C}_0$ is positive for all κ. Values of $\mathscr{C}_0$ for the experiments in Japan and the Antarctic are given in table 4.

With our choice of eigenvectors and generalized eigenvectors, the projection Π of w on the invariant subspace spanned by $\varphi_0^+, \varphi_0^-, \varphi_1^+, \varphi_1^-$ is given by

$$\Pi(w) = \langle w, \psi_+^0 \rangle \varphi_0^+ + \langle w, \psi_+^1 \rangle \varphi_1^+ + \langle w, \psi_-^0 \rangle \varphi_0^- + \langle w, \psi_-^1 \rangle \varphi_1^-.$$

The coefficient q_2 is obtained by taking the scalar product of (4.26) with ψ_+^1:

$$q_2 = -\langle 2N_2(\varphi_0^+, \Phi_{1100}) + 2N_2(\varphi_0^-, \Phi_{2000}) + 3N_3(\varphi_0^+, \varphi_0^+, \varphi_0^-), \psi_+^1 \rangle. \tag{4.28}$$

All the symbolic computations needed to find $\Phi_{1100}, \Phi_{2000}, q_2$ and the nonlinear terms $N_2(w, w)$, $N_3(w, w, w)$ are performed using the software MAPLE. The expressions for Φ_{1100} and Φ_{2000}, which are obtained from (4.25) and (4.24), read

$$\Phi_{1100} = \begin{pmatrix} 0 \\ 2K \tanh \kappa \\ 0 \\ 0 \\ \left(\dfrac{\lambda}{\lambda - 1}\right) \dfrac{\sinh 2\kappa + \kappa}{\kappa \cosh^2 \kappa} \end{pmatrix}, \quad \Phi_{2000} = \begin{pmatrix} -i\mathscr{A} \\ K(2\mathscr{A} + \tanh \kappa) \\ iK^2(4\mathscr{A} + 3 \tanh \kappa) \\ -i\mathscr{A} \sinh 2(K\psi + \kappa)/\sinh 2\kappa \\ \mathscr{A} \cosh 2(K\psi + \kappa)/\sinh 2\kappa \end{pmatrix},$$

where

$$\mathscr{A} = 3 \sinh \kappa \left(\frac{5\kappa - \sinh \kappa \cosh \kappa}{-15\kappa \cosh \kappa + 15 \sinh \kappa + 11 \sinh^3 \kappa} \right). \tag{4.29}$$

All values of λ are taken along the curve (4.13). The asymptotic behaviour of $\mathscr{A}$ is

$$\mathscr{A} \to -\tfrac{3}{11} \text{ as } \kappa \to \infty, \quad \mathscr{A} \sim \frac{2}{\kappa} - \tfrac{5}{3}\kappa + O(\kappa^2) \text{ as } \kappa \to 0.$$

The values of $\mathscr{A}$ corresponding to the two sets of experiments are given in table 4. The expression (4.28) for q_2 is

$$q_2(\kappa) = \frac{\mathscr{C}_0}{8\kappa^2(\lambda - 1) \sinh^2 \kappa \cosh^3 \kappa}$$
$$\times \{12\mathscr{A}(\lambda - 1)\kappa \cosh^3 \kappa(\kappa^2 - \kappa \sinh \kappa \cosh \kappa + \lambda \sinh^2 \kappa)$$
$$-\kappa^3 \sinh \kappa[(11 \sinh^2 \kappa + 8) - \lambda(11 \sinh^2 \kappa + 12)]$$
$$-\kappa^2 \sinh^2 \kappa \cosh \kappa[\lambda(11 \sinh^2 \kappa - 8) - (11 \sinh^2 \kappa + 4)]$$
$$+4\kappa \sinh^3 \kappa(3 + \sinh^2 \kappa)\lambda(\lambda + 1) + 32\lambda^2 \sinh^4 \kappa \cosh \kappa\}. \tag{4.30}$$

The coefficient $q_2(\kappa)$ is plotted in figure 6. It is a monotonically decreasing function of κ, with the following asymptotic behaviour:

$$q_2 \sim \tfrac{57}{4} 6^{1/3} \kappa^{-10/3} + O(\kappa^{-4/3}) \text{ as } \kappa \to 0, \quad q_2 \to -\tfrac{79}{528} 4^{1/3} \approx -0.2375 \text{ as } \kappa \to \infty.$$

It vanishes for $\kappa \approx 5.79$ (the corresponding values of λ and f given by (4.13) are 4.34 and 0.473 as shown in figure 5). The values of q_2 corresponding to the two sets of experiments are given in table 4 and shown in figure 6. One can link the vanishing of q_2 with a critical fluid depth. Below that critical depth, q_2 is negative; above, it is positive. The critical depths for both sets of experiments are indicated in table 4.

Now that we have computed the coefficients q_1 and q_2, we go back to the system (4.18)–(4.19). Let $\tilde{A} = Ae^{-iK\phi}, \tilde{B} = Be^{-iK\phi}$. At leading order, the system (4.18)–(4.19) becomes

$$\tilde{A}_\phi = \tilde{B} + \cdots, \tag{4.31}$$
$$\tilde{B}_\phi = \tilde{A}(q_1\mu - q_2|\tilde{A}|^2) + \varepsilon e^{-iK\phi} p_0 \mathscr{C}_0 + \cdots. \tag{4.32}$$

Since $\phi_x = u = e^\beta \cos \alpha \approx 1$ at leading order, the potential ϕ can be replaced by x, so that our problem is finally reduced to the forced nonlinear Schrödinger (NLS) equation:

$$\tilde{A}_{xx} = q_1\mu\tilde{A} - q_2\tilde{A}|\tilde{A}|^2 + \tilde{\varepsilon}\delta, \tag{4.33}$$

where

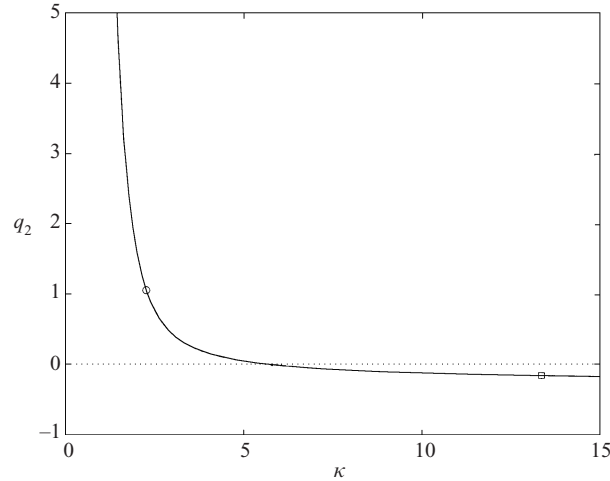$$\tilde{\varepsilon} = \mathscr{C}_0 \varepsilon \int_{-\infty}^{\infty} p_0(x)\mathrm{d}x$$

FIGURE 6. Plot of the coefficient q_2 given by (4.30) versus κ. Large values of κ correspond to deep water. Small values of κ correspond to shallow water. The circle corresponds to Takizawa's experiments, the square to the Antarctic experiments while the dot corresponds to the vanishing of q_2.

(see equation (4.27) for the expression for $\mathscr{C}_0$). If the load-induced pressure has the same expression as in §3, then $\tilde{\varepsilon} = \mathscr{C}_0 \, P/\rho U^2$. For positive P, $\tilde{\varepsilon}$ is positive. More details on the derivation of the forced NLS equation can be found in Părău & Dias (2000). The next section is devoted to solutions of (4.33). Once solutions for $\tilde{A}$ have been found, one can compute $A = \tilde{A}\mathrm{e}^{\mathrm{i}Kx}$ and $B = \tilde{A}_x\mathrm{e}^{\mathrm{i}Kx}$. At leading order, the solution w of (4.9) is given by $w = A\varphi_0^+ + \bar{A}\varphi_0^-$, that is

$$
\begin{pmatrix} \alpha_0 \\ V \\ W \\ \alpha \\ \beta \end{pmatrix} = \frac{A}{\cosh\kappa} \begin{pmatrix} \mathrm{i}\sinh\kappa \\ -K\sinh\kappa \\ -\mathrm{i}K^2\sinh\kappa \\ \mathrm{i}\sinh(K\psi + \kappa) \\ -\cosh(K\psi + \kappa) \end{pmatrix} + \frac{\bar{A}}{\cosh\kappa} \begin{pmatrix} -\mathrm{i}\sinh\kappa \\ -K\sinh\kappa \\ \mathrm{i}K^2\sinh\kappa \\ -\mathrm{i}\sinh(K\psi + \kappa) \\ -\cosh(K\psi + \kappa) \end{pmatrix}. \quad (4.34)
$$

Using (4.6), it follows that the ice-sheet deflection reads

$$
\eta = -\frac{\lambda}{f}[\beta] = \frac{\tanh\kappa}{K}(A + \bar{A}) = \frac{\tanh\kappa}{K}(\tilde{A}\mathrm{e}^{\mathrm{i}Kx} + \text{c.c.}). \quad (4.35)
$$

5. Solutions of the forced nonlinear Schrödinger equation

In order to study the solutions of the forced NLS equation (4.33), it is convenient to study first the solutions without forcing, i.e. with $\tilde{\varepsilon} = 0$ in (4.33). Let us write

$$
\tilde{A}(x) = s(x)\mathrm{e}^{\mathrm{i}\theta(x)},
$$

separate real and imaginary parts and integrate the equation. After some calculations, one finds that s, or rather $u = s^2$, and θ satisfy the equations

$$
\tfrac{1}{4}u_x^2 = q_1\mu u^2 - \tfrac{1}{2}q_2 u^3 - I^2 + Hu, \quad u\theta_x = I. \quad (5.1)
$$

The solutions are completely characterized by the two first integrals I and H. These two integrals are related to the energy flux and flow force. Since only speeds U less than $c_{\min}$ are considered, the parameter μ introduced in (4.14) is always positive. Then
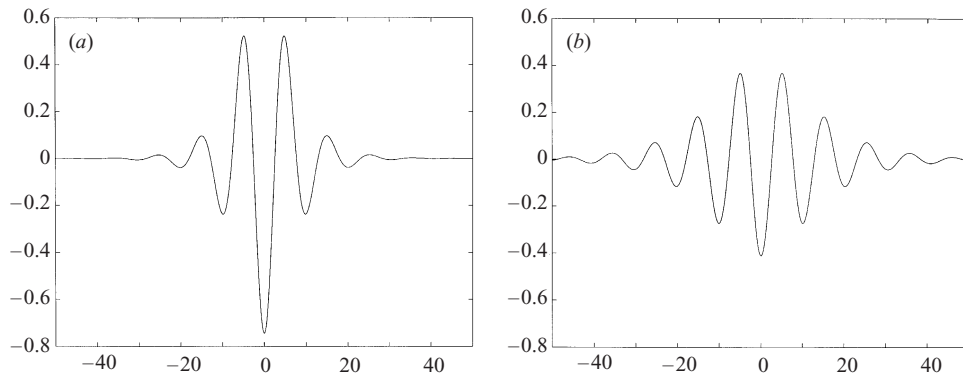
FIGURE 7. Plot of the ice-sheet deflection $\eta(x)$ (see equation (5.3)) for two solitary waves of depression. Except for the pressure load, which is absent, the parameters are the same as in Takizawa's experiments. (*a*) $U = 5.8\,\text{m}\,\text{s}^{-1}$, i.e. $f = 0.552$ and $\lambda = 1.98$. Consequently, $\kappa = 2.19$ and $\mu = 0.065$. The unit length is $L = 1.9\,\text{m}$. (*b*) $U = 6\,\text{m}\,\text{s}^{-1}$, i.e. $f = 0.504$ and $\lambda = 1.85$. Consequently, $\kappa = 2.25$ and $\mu = 0.019$. The unit length is $L = 1.85\,\text{m}$.

there are two cases to consider. If $q_2 < 0$, there are no bounded solutions. If $q_2 > 0$, there are periodic solutions (of finite amplitude only), quasi-periodic solutions and solitary waves, tending to zero at infinity (see Iooss & Adelmeyer 1992). For these solitary waves, the expression for s is

$$s(x) = \pm \sqrt{\frac{2\mu q_1}{q_2}} \left(\frac{1}{\cosh(\sqrt{\mu q_1}x)} \right), \tag{5.2}$$

and θ is a constant. The corresponding ice-sheet deflection (4.35) is

$$\eta = \pm \frac{2\tanh\kappa}{K} \sqrt{\frac{2\mu q_1}{q_2}} \frac{\cos(Kx)}{\cosh(\sqrt{\mu q_1}x)}. \tag{5.3}$$

In physical variables, this expression becomes

$$\zeta(x^*, t) = \pm \frac{2\tanh(kH)}{k} \sqrt{\frac{2\mu q_1}{q_2}} \frac{\cos[k(x^* + Ut)]}{\cosh[\sqrt{\mu q_1}(x^* + Ut)/L]}. \tag{5.4}$$

Two solitary waves of depression have been plotted in figure 7 (at leading order, the wave of elevation is just the mirror image of the depression wave). The parameters H and D are those of the experiments in Japan. The amplitudes $|\zeta(0)|$ of the waves are approximately 1.4 m and 76 cm. They are almost two orders of magnitude larger than the amplitude of the waves shown in figure 4. These waves are not realistic and definitely violate the assumptions made in the present theory. But recall that the comparison is misleading at this stage because the wave shape (5.4) was obtained without forcing.

Now let us reintroduce the forcing ($\tilde{\varepsilon} \neq 0$). Although the solution of the linearized problem becomes singular when $\mu \to 0$ due to the 1:1 resonance, the finite-amplitude response close to resonant conditions is bounded. In that case, one can obtain solitary wave type profiles even if $q_2 < 0$.

We look for solutions of (4.33) which are continuous and bounded for $x \in \mathbb{R}$, satisfy $\tilde{A}_{xx} = q_1 \mu \tilde{A} - q_2 \tilde{A}|\tilde{A}|^2$ for $x \neq 0$, and $\tilde{A}_x(0+) - \tilde{A}_x(0-) = \tilde{\varepsilon}$. Moreover we restrict the analysis to solitary waves tending to zero at infinity.

The analysis is the same as before, except that now equation (5.1) must be written separately for $x < 0$ and for $x > 0$:

$$\tfrac{1}{4}u_x^2 = q_1\mu u^2 - \tfrac{1}{2}q_2 u^3 - I_1^2 + H_1 u, \quad u\theta_x = I_1, \quad x < 0,$$

$$\tfrac{1}{4}u_x^2 = q_1\mu u^2 - \tfrac{1}{2}q_2 u^3 - I_2^2 + H_2 u, \quad u\theta_x = I_2, \quad x > 0.$$

The constants I_1, I_2, H_1, H_2 are chosen to be zero in order to obtain solitary waves tending to zero at infinity. Then necessarily $\sin(\theta(0)) = 0$ and $s_x(0+) = -s_x(0-) = \tilde{\varepsilon}/2$.

For the experiments in Japan, $q_1 > 0$ and $q_2 > 0$ (see table 4). Solitary waves can only be obtained for positive μ, i.e. $U < c_{\min}$. Let

$$\mu^* = \frac{1}{q_1}\sqrt{\frac{q_2}{2}}\tilde{\varepsilon}.$$

For Takizawa's experiments, $\tilde{\varepsilon} \approx 0.0026$, so that $\mu^* \approx 0.004$. Consequently $U^* = 6.06\,\mathrm{m\,s^{-1}}$. There are four solitary waves for $\mu > \mu^*$, two of elevation and the other two of depression. One elevation wave and one depression wave are perturbations of the waves (5.3) found without the forcing. The other depression wave is a perturbation of the linearized solution found in §3. The other elevation wave does not relate to previous solutions. If $\mu = \mu^*$, there are only two solutions, one being an elevation solitary wave and the other one a depression solitary wave. For $0 \leqslant \mu < \mu^*$, there are no solitary waves.

In the general case, the solutions can be written as

$$s(x) = \pm\sqrt{\frac{2\mu q_1}{q_2}}\left(\frac{1}{\cosh(\sqrt{\mu q_1}|x| \mp \alpha_{1/2})}\right), \tag{5.5}$$

where α_1 and α_2 are the solutions of

$$\frac{\sinh\alpha}{\cosh^2\alpha} = \frac{\sqrt{q_2}}{2\sqrt{2}q_1}\left(\frac{\tilde{\varepsilon}}{\mu}\right).$$

The corresponding wave profiles (4.35) are given by

$$\eta(x) = 2K^{-1}\tanh\kappa s(x)\cos(Kx). \tag{5.6}$$

The four solutions (5.5) as well as the corresponding profiles (5.6) are shown in figure 8. Clearly the only physically acceptable solution is the small-amplitude depression wave. It is interesting to note that recent stability results of Calvo & Akylas (2002) seem to indicate that the small-amplitude depression wave is the only one which is stable.

For the Antarctic experiments, $q_1 > 0$ and $q_2 < 0$ (see table 4). A unique solitary wave can be found for all positive values of μ, as opposed to the case without forcing, where no solitary waves could be found. It is a depression solitary wave, which can be viewed as a perturbation of the linearized solution of §3. The solution can be expressed as

$$s(x) = -\sqrt{\frac{2\mu q_1}{|q_2|}}\left(\frac{1}{\sinh(\sqrt{\mu q_1}|x| + \alpha)}\right),$$

where α is the single positive root of the equation

$$\frac{\cosh\alpha}{\sinh^2\alpha} = \frac{\sqrt{|q_2|}}{2\sqrt{2}q_1}\left(\frac{\tilde{\varepsilon}}{\mu}\right).$$

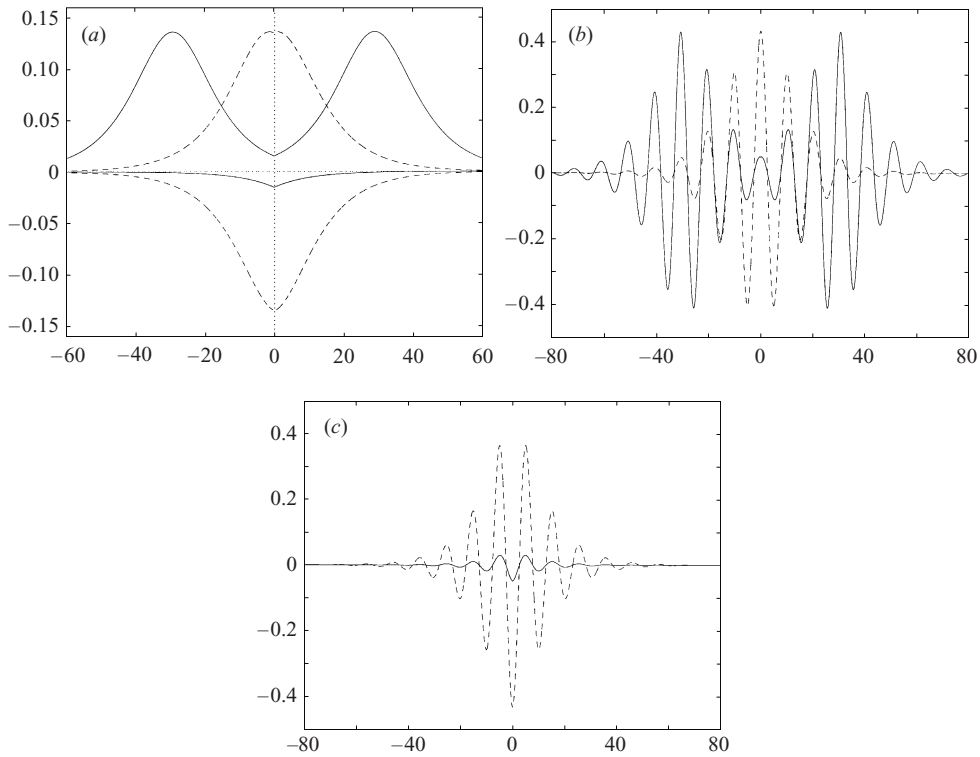The corresponding wave profile (4.35) is again given by (5.6) and is plotted in figure 9.

FIGURE 8. Solutions of the forced NLS equation in relatively shallow water ($q_2 > 0$). This case corresponds to the experiments in Japan. The parameters are $\tilde{\varepsilon} = 0.003$, $\mu = 0.02$ (i.e. $U \approx 6\,\mathrm{m\,s^{-1}}$), $\kappa = 2.27$. (*a*) The profiles $s(x)$ given by (5.5). (*b*) The corresponding wave profiles $\eta(x)$ for the elevation waves. (*c*) The corresponding wave profiles $\eta(x)$ for the depression waves.
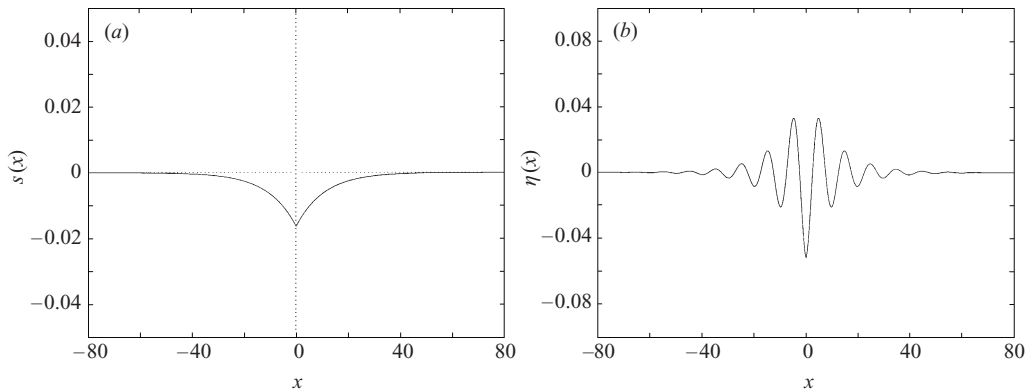

FIGURE 9. Solutions of the forced NLS equation in deep water ($q_2 > 0$). This case corresponds to the Antarctic experiments. The parameters are $\tilde{\varepsilon} = 0.003$, $\mu = 0.02$, $\kappa = \infty$ (infinite depth). Plot of the profile $s(x)$ (*a*) and of the corresponding wave profile $\eta(x)$ (*b*).

For $\mu = 0$, there is also a depression solitary wave, but it decays algebraically at infinity, as opposed to the previous cases where the solutions were decaying exponentially:

$$s(x) = -\frac{1}{(\frac{1}{2}|q_2|)^{1/2}|x| + (\tilde{\varepsilon}^{-1}\sqrt{2|q_2|})^{1/2}}.$$
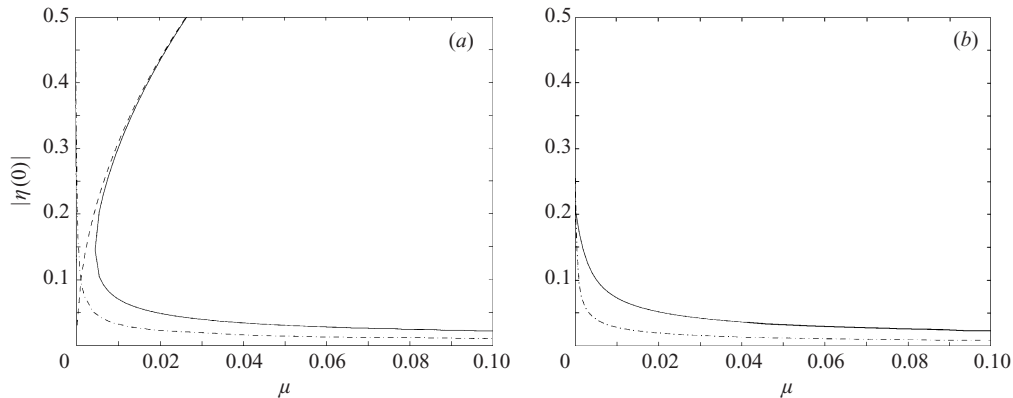
FIGURE 10. The amplitude $|\eta(0)|$ as a function of μ for $q_2 > 0$ (a) and $q_2 < 0$ (b). The value of κ is 2.27 for $q_2 > 0$, as in figure 8. The value of κ is infinity for $q_2 < 0$, as in figure 9. Various solutions are shown: the solution of the linearized problem ($\cdot - \cdot - \cdot$) with $\tilde{\varepsilon} \neq 0$ (see §3), the analytical solution with $\tilde{\varepsilon} = 0$ (——) and the solutions of the forced nonlinear Schrödinger equation (4.33) with $\tilde{\varepsilon} \neq 0$ (solid line). When $q_2 < 0$, $|\eta(0)|$ remains finite in the limit $\mu \to 0$. When $\tilde{\varepsilon} \neq 0$, its value is 0.003 in the plots.

Figure 10 shows the amplitude at the origin of the various linear and nonlinear analytical solutions which have been computed in this paper. From figure 10, one may conclude the following. In all water depths, the linearized theory is sufficient to describe the observed phenomena, i.e. the existence of a solitary wave of depression, for speeds not too close to $c_{\min}$ (say $\mu > 0.05$). For $0 \leqslant \mu < 0.05$, the weakly nonlinear theory predicts the fate of this solitary wave of depression. In large water depth ($q_2 < 0$), it persists all the way to $c_{\min}$ and its amplitude remains realistic. For the Antarctic experiments, we do not have direct access to the ice-sheet deflection but weakly nonlinear theory and experiments agree qualitatively. In small water depth, the depression wave ceases to exist at $U^* < c_{\min}$. In the experiments in Japan, in relatively shallow water, the solitary wave of depression seems to have been observed all the way to $U = c_{\min}$, in apparent contradiction with the present results. However, the theoretical value of $U^* = 6.06\,\mathrm{m\,s^{-1}}$ is so close to $U = c_{\min} = 6.09\,\mathrm{m\,s^{-1}}$ that one has to be cautious in interpreting the experimental as well as the theoretical results. The next section is devoted to a more complete discussion.

6. Discussion

Comparing theory and experiments is always a difficult task. In the case of ice-sheet deflections induced by a moving load, this task is particularly difficult because many effects come into play. First, the modelling of ice is not an easy task. In our model, the ice acceleration term has been neglected. This can be justified provided the wavelength of the surface displacement is much larger than the ice thickness. Since the water motion penetrates to a depth comparable with one wavelength, the inertia of the thin ice plate will thus be small compared with that of the moving-water layer. The ice thickness has been neglected in our model, based on the justification given by Strathdee *et al.* (1991): thin-plate theory is accurate to within 5% for distances greater than twenty times the ice thickness. Another effect which may play a role in the dynamics of waves in the ice layer is the compressibility of water as shown by Brevdo (2001). Another source of error in the

comparison between theory and experiments is the modelling of the load-induced pressure. In the experiments, the load is clearly two-dimensional, while our model is one-dimensional. Dissipative forces may also play a role in the experiments. In the literature so far, only the effect of damping has been used to explain why the deflection of ice sheets does not go to infinity as U approaches c_{min}. Takizawa (1987) and Hosking *et al.* (1988) studied the effect of viscosity on the linearized problem and concluded that the classical model for the steady-state behaviour fails at $U = c_{min}$ owing to its neglect of dissipative effects. When physical damping is included in the calculations, the integrals do not diverge near the critical speed.

Putting these comments aside, let us now concentrate on the results of this paper. If nonlinear effects are important near c_{min}, then the behaviour depends on water depth, if we keep the other physical parameters constant. For Takizawa's experiments, the water is relatively shallow. Theoretically, we found a transition region for speeds slightly less than c_{min}, where no steady solutions in the form of solitary waves exist. This transition region is different from the transition regions that Takizawa (1985) introduces: the latter are based on qualitative behaviour of the deflection of the ice sheet for speeds less than c_{min}. We believe that the transitional speed U^* being so close to c_{min} explains why solitary waves have been observed all the way to the critical speed c_{min}. In shallower water, one may be able to observe a clear transition region, i.e. a region without steady solutions. In infinite depth, there is no transition region and steady solutions exist all the way to c_{min}. Our conclusion is that the solutions are described adequately by the forced nonlinear Schrödinger equation when the speed U is close to c_{min}, while for $U \ll c_{min}$ the linearized equations are adequate.

Previously it was established that dissipative effects are the main explanation for making the ice deflection finite near c_{min}. In the present paper, we have shown that nonlinear effects are another possible explanation. It is fair to say that most probably nonlinear effects compete with dissipative effects in order to make the ice deflection finite as U tends to c_{min}. However, our weakly nonlinear theory cannot yet explain the observed lag of the position of maximum depression immediately behind the load. It is possible to combine nonlinearity and damping in a nonlinear Schrödinger equation where damping is introduced artificially. This technique was used by Barnard, Mahony & Pritchard (1977) in their study of surface waves near a cut-off frequency.

The focus of the present paper has been the critical speed c_{min}. But there is another critical speed, the speed of gravity waves on shallow water c_0, at which nonlinear effects probably play a role. This is left for a future study.

Appendix. Numerical results

The main purpose of this Appendix is to show that the weakly nonlinear theory developed in §4 is valid for cases of physical interest. Solitary wave solutions of the full Euler equations (4.1)–(4.4) without forcing are computed numerically and compared with the weakly nonlinear solutions. Equations (4.1)–(4.4) are rewritten in

terms of the velocity potential:

$$\phi_{xx} + \phi_{yy} = 0, \quad (x, y) \in \mathbb{R} \times [-\lambda/f, \eta(x)], \quad \text{(A 1)}$$

$$\phi_y = 0 \quad \text{at } y = -\lambda/f, \quad \text{(A 2)}$$

$$\phi_x \eta_x - \phi_y = 0 \quad \text{at } y = \eta(x), \quad \text{(A 3)}$$

$$\tfrac{1}{2}(\phi_x^2 + \phi_y^2 - 1) + f\eta + \partial_{xx}^2 \frac{\eta_{xx}}{(1 + \eta_x^2)^{3/2}} = 0 \quad \text{at } y = \eta(x). \quad \text{(A 4)}$$

Again the independent variable is the complex potential $\mathscr{F}(z) = \phi + i\psi$, where $z = x + iy$. As before, we choose $\psi = 0$ along the bottom of the ice sheet. Moreover, ϕ is chosen to be 0 at $x = 0$. Then

$$\phi_x - i\phi_y = \frac{d\mathscr{F}}{dz} = \frac{1}{x'(\phi) + i\eta'(\phi)},$$

where $x'(\phi)$ and $\eta'(\phi)$ are the values of $dx/d\phi$ and $dy/d\phi$ evaluated on the bottom of the ice sheet $\psi = 0$. Bernoulli's equation becomes

$$\frac{1}{2}\left(\frac{1}{x'^2 + \eta'^2} - 1\right) + f\eta + \frac{S}{x'^3(x'^2 + \eta'^2)^{7/2}} = 0, \quad \text{(A 5)}$$

where

$$\begin{aligned}
S = {}& -x'\eta'^5 x^{(iv)} - 3x''^2\eta'^4\eta'' + x''\eta'^5 x''' - 2x'^3\eta'^3 x^{(iv)} - 4x'^5\eta'' x''' + 2x'^4\eta^{(iv)}\eta'^2 \\
& + x'^2\eta^{(iv)}\eta'^4 + 15\eta'' x'^4 x''^2 + 12\eta''^3 x'^2\eta'^2 - 15\eta' x''^3 x'^3 + x'^6\eta^{(iv)} - 6\eta''' x'^5 x'' \\
& - x'^5\eta' x^{(iv)} - 3x'^4\eta''^3 - 33\eta'^2 x''^2 x'^2\eta'' - 9\eta''' x'^4\eta'\eta'' - 3\eta''' x'^3\eta'^2 x'' \\
& - 9\eta''' x'^2\eta'^3\eta'' + 10\eta' x''' x'^4 x'' + \eta'^2 x''' x'^3\eta'' + 11\eta'^3 x''' x'^2 x'' + 36\eta''^2 x'^3 x''\eta' \\
& + 5x'\eta'^4 x'''\eta'' - 9x'\eta'^3 x''\eta''^2 + 3x'\eta''' x''\eta'^4.
\end{aligned}$$

By using Cauchy's formula in order to calculate $x'(\phi) + i\eta'(\phi) - 1$ for a point ϕ along the bottom of the ice sheet, one obtains the integro-differential equation

$$\begin{aligned}
x'(\phi) - 1 = {}& -\frac{1}{\pi} \int_0^\infty \eta'(s)\left(\frac{1}{s - \phi} + \frac{1}{s + \phi}\right) ds \\
& + \frac{f}{\pi} \int_0^\infty \frac{f(\phi - s)\eta'(s) + 2\lambda(x'(s) - 1)}{f^2(s - \phi)^2 + 4\lambda^2} ds \\
& + \frac{f}{\pi} \int_0^\infty \frac{-f(\phi + s)\eta'(s) + 2\lambda(x'(s) - 1)}{f^2(s + \phi)^2 + 4\lambda^2} ds. \quad \text{(A 6)}
\end{aligned}$$

Equations (A 5) and (A 6) define a system for the unknown functions $x(\phi)$ and $\eta(\phi)$ which is solved by the method described in Dias, Menasce & Vanden-Broeck (1996). The system is discretized by choosing N equally-spaced point $\phi_i = i\Delta\phi$ for the potential. The spacing $\Delta\phi$ is a crucial parameter for the accuracy of the numerical computations. The system is then solved by Newton's method for given values of f and λ.

The number of points used for solving these equations was 800 in most cases and the length of the discretization interval was $\Delta\phi = 0.05$. As the velocity approaches $c_{\min}$, the oscillations become more visible as their decay becomes slower. We restricted our numerical computations to the branches predicted by the dynamical system analysis of §4. A wave of depression as well as a wave of elevation are shown in figure 11. The values of D and H are those of Takizawa's experiments. The analytical profiles are shown for comparison. The effect of truncation can be seen, especially
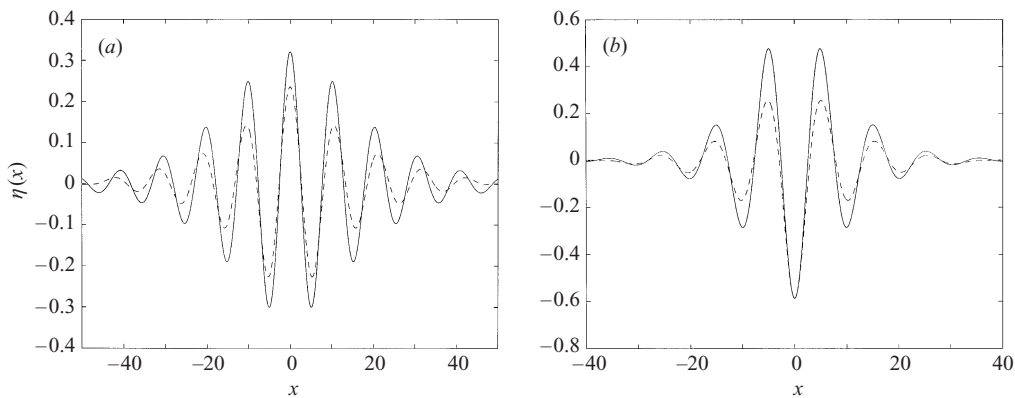
FIGURE 11. Profiles $\eta(x)$ of an elevation solitary wave (*a*) with $f = 0.4959$, $\lambda = 1.838$, $\mu = 0.018$ and of a depression solitary wave (*b*) with $f = 0.5215$, $\lambda = 1.933$, $\mu = 0.036$. For these two waves, the ratio f/λ is equal to 0.27. The solid line is the analytical solution. The dashed line is the numerical solution.

for the elevation wave. Since there is no uniqueness we observed that the schema is sensitive to the initial guess. As in the problem of capillary–gravity waves, we expect a plethora of solutions. The branches predicted by the dynamical system analysis of §4 are modulated wave packets whose envelopes are symmetric and decay exponentially to zero at infinity. In the middle, one wave has a central crest (elevation wave), while the other wave has a central trough (depression wave). As shown in §4, the normal form (4.18)–(4.19) yields the NLS equation to leading order. And the NLS equation admits two symmetric envelope-soliton solutions. But one can also construct small-amplitude asymmetric solitary waves, by translating the crests of a symmetric solitary wave relative to its wave envelope. The problem is that such asymmetric waves do not persist when considering the full system. Exponentially small terms come into play. Shifting the carrier oscillations relative to the envelope leads to the appearance of growing oscillations of exponentially small amplitude on one side of the wavepacket. However, due to nonlinearity, this growing tail evolves into a new wavepacket and it can be shown that, for certain values of the phase of the carrier oscillations, the whole disturbance terminates, resulting in a solitary wave with two wavepackets. Otherwise, a third wavepacket is generated and the process continues. The main result is that there exists a countable infinity of symmetric and asymmetric multibump solutions. But, unlike the solitary waves obtained in §5, which bifurcate from the rest state, each of these multibump solitary waves bifurcates at a certain finite amplitude.

  Although it is easy to add a pressure disturbance to equation (A 4), as was done by Vanden-Broeck & Dias (1992) for capillary–gravity waves, we did not do it for the following reason: we have showed that even for relatively small values of μ ($\mu \approx 10^{-2}$), the deflection of the floating ice sheet in the absence of a moving load is rather large (≈ 60 cm in the conditions of the experiments in Japan). Therefore, only very small values of μ are of interest physically to study nonlinear effects. For larger values of μ, the linearized theory is sufficient to describe the observed phenomena. But for small values of μ, the weakly nonlinear results are adequate and it is not necessary to compute solutions of the full equations, even in the presence of a moving load.

REFERENCES

ASHTON, G. D. 1986 *River and Lake Ice Engineering*, Water Resources Publications, Littleton, Colorado.

BARNARD, B. J. S., MAHONY, J. J. & PRITCHARD, W. G. 1977 The excitation of surface waves near a cut-off frequency. *Phil. Trans. R. Soc. Lond.* A **286**, 87–123.

BREVDO, L. 2001 Resonant destabilization of a floating homogeneous ice layer. *Z. Angew. Math. Phys.* **52**, 397–420.

CALVO, D. C. & AKYLAS, T. R. 2002 Stability of steep gravity–capillary solitary waves in deep water. *J. Fluid Mech.* **452**, 123–143.

DAVYS, J. W. HOSKING, R. J. & SNEYD, A. D. 1985 Waves due to a steadily moving source on a floating ice plate. *J. Fluid Mech.* **158**, 269–287.

DIAS, F. & IOOSS, G. 1993 Capillary–gravity solitary waves with damped oscillations. *Physica* D **65**, 399–423.

DIAS, F. & IOOSS, G. 2003 Water waves as a dynamical system. In *Handbook of Mathematical Fluid Dynamics*, vol. 2. Elsevier (to appear).

DIAS, F. & KHARIF, C. 1999 Nonlinear gravity and capillary–gravity waves. *Annu. Rev. Fluid Mech.* **31**, 301–346.

DIAS, F., MENASCE, D. & VANDEN-BROECK, J.-M. 1996 Numerical study of capillary–gravity solitary waves. *Euro. J. Mech.* B/*Fluids* **15**, 17–36.

FORBES, L. K. 1986 Surface waves of large amplitude beneath an elastic sheet. Part 1. High-order series solution. *J. Fluid Mech.* **169**, 409–428.

HOSKING, R. J., SNEYD, A. D. & WAUGH, D. W. 1988 Viscoelastic response of a floating ice plate to a steadily moving load. *J. Fluid Mech.* **196**, 409–430.

IL'ICHEV, A. 2000 Solitary waves in media with dispersion and dissipation (A review). *Fluid Dyn.* **35**, 157–176.

IOOSS, G. & ADELMEYER, M. 1992 *Topics in Bifurcation Theory and Applications*. World Scientific.

KHEYSIN, D. YE. 1963 Moving load on an elastic plate which floats on the surface of an ideal fluid. *Izv. Akad. Nauk SSSR, Otd. Tekh. Nauk, Mekh. i Mashinostroenie* **1**, 178–180 (in Russian).

KIRCHGÄSSNER, K. 1988 Nonlinearly resonant surface waves and homoclinic bifurcation. *Adv. Appl. Mech.* **26**, 135–181.

LEVI-CIVITA, T. 1925 Détermination rigoureuse des ondes permanentes d'ampleur finie. *Math. Annalen* **93**, 264–314.

LONGUET-HIGGINS, M. S. & ZHANG, X. 1997 Experiments on capillary–gravity waves of solitary type on deep water. *Phys. Fluids* **9**, 1963–1968.

MIELKE, A. 1986 Steady flows of inviscid fluids under localized perturbations. *J. Diffl Equat.* **65**, 89–116.

MILINAZZO, F., SHINBROT, M. & EVANS, N. W. 1995 A mathematical analysis of the steady response of floating ice to the uniform motion of a rectangular load. *J. Fluid Mech.* **287**, 173–197.

NEVEL, D. E. 1970 Moving loads on a floating ice sheet. *CRREL Res. Rep.* 261. US Army Cold Regions Research and Engineering Laboratory, Hanover, NH, USA.

PEAKE, N. 2001 Nonlinear stability of a fluid-loaded elastic plate with mean flow. *J. Fluid Mech.* **434**, 101–118.

PĂRĂU, E. & DIAS, F. 2000 Ondes solitaires forcées de capillarité-gravité. *C. R. Acad. Sci. Paris* I **331**, 655–660.

SCHULKES, R. M. S. M. & SNEYD, A. D. 1988 Time-dependent response of floating ice to a steadily moving load. *J. Fluid Mech.* **186**, 25–46.

SQUIRE, V. A., ROBINSON, W. H., LANGHORNE, P. J. & HASKELL. T. G. 1988 Vehicles and aircraft on floating ice. *Nature* **333**, 159–161.

SQUIRE, V. A., HOSKING, R. J., KERR, A. D. & LANGHORNE, P. J. 1996 *Moving Loads on Ice Plates*. Kluwer.

STRATHDEE, J., ROBINSON, W. H., & HAINES, E. M. 1991 Moving loads on ice plates of finite thickness. *J. Fluid Mech.* **226**, 37–61.

TAKIZAWA, T. 1985 Deflection of a floating sea ice sheet induced by a moving load. *Cold Regions Sci. Tech.* **11**, 171–180.

Takizawa, T. 1987 Field studies on response of a floating sea ice sheet to a steadily moving load. *Contrib. Inst. Low Temp. Sci.* A **36**, 31–76.

Takizawa, T. 1988 Response of a floating sea ice sheet to a steadily moving load. *J. Geophys. Res.* **93**, 5100–5112.

Vanden-Broeck, J.-M. & Dias, F. 1992 Gravity–capillary solitary waves in water of infinite depth and related free-surface flows. *J. Fluid Mech.* **240**, 549–557.